

Optimization Problem of Multibeam Bathymetry Based on Analytical Geometry

Jieyan Han^{1,a}, Xiaoyu Zheng^{1,b}

¹School of Mathematics and Computer Science, Yan'an University, Yan'an, Shaanxi, China
^ajiexianhan2023@163.com, ^bxiaoyuzheng0411@163.com

Abstract: Multibeam bathymetry technology finds extensive applications in underwater depth exploration. This paper focuses on constructing a concrete mathematical model for the multibeam bathymetry problem, conducting research, and discussions. The developed model is applied to address the route planning issue for multibeam survey systems in seabed exploration. Initially, we employ mathematical methods from analytical geometry to establish a mathematical model concerning the coverage width and overlap rate between adjacent swathes in multibeam bathymetry. We compute the corresponding indicator values based on this model. Subsequently, utilizing the mathematical model in conjunction with an enumeration method, we design a set of survey lines that satisfy overlap rate requirements, minimize measurement lengths, and completely cover the entire target area. Finally, an optimization model is constructed for the survey layout of the bathymetric measurement vessel, meeting the specified criteria. The result is an optimized multibeam survey layout design. The proposed model aligns well with practical considerations, offering a rational solution to the posed problem. It demonstrates practical utility, algorithmic intuitiveness, and is pertinent in the field of marine exploration.

Keywords: Multibeam Bathymetry Technology, Analytical Geometry, Enumeration Method, Optimization Model

1. Introduction

When it comes to measuring water depth, multibeam bathymetry technology is a widely used method. This technique employs multiple sonar beams to simultaneously scan the underwater terrain, determining the shape and depth of the underwater topography by calculating the propagation time and reflection intensity of sound waves. Compared to traditional single-beam bathymetry techniques, multibeam bathymetry technology offers higher measurement accuracy and a broader measurement range. Consequently, it has found extensive applications in marine exploration, seabed topographic mapping, navigation safety, and other fields.

In recent years, significant progress has been made in the application of multibeam bathymetry systems in marine research. Brown et al. (2011) reviewed research advancements in mapping seafloor habitats using acoustic technology to enhance understanding of underwater spatial ecology [1]. Mitchell et al. (2018) explored the optimization of multibeam echo sounder seabed echo data acquisition and processing techniques to improve detection and mapping capabilities for deep-water oil and gas leaks [2]. Lucieer et al. (2018) focused on user expectations for multibeam echo sounder echo intensity data and speculated about future developments [3]. Hughes Clarke (2016) first demonstrated the connection between sediment dynamics and flow features in wide-angle views [4]. Lamarche et al. (2011) quantitatively analyzed the seafloor topography of the Cook Strait in New Zealand using multibeam echo sounder data [5]. Pratomo and Saputro (2021) conducted a comparative analysis of bathymetric data from single-beam and multibeam echo sounders [6]. Weber et al. (2018) proposed a standard line method for calibrating multibeam echo sounders [7]. Parnum and Gavrillov (2011) studied the measurement of seafloor echoes by high-frequency multibeam echo sounders in shallow water, with a focus on data acquisition and processing [8]. Snellen et al. (2018) assessed the performance of classification methods based on multibeam echo sounder data in monitoring the distribution of seafloor sediments [9]. Roche et al. (2018) explored the control of repeatability in high-frequency multibeam echo sounder echo data using natural reference areas [10].

This paper primarily focuses on constructing a specific mathematical model for the multibeam bathymetry problem and conducting research and discussions. The study aims to achieve the desired

target results through variations in parameters.

2. Models and Methods

In order to calculate the coverage width and overlap rate between adjacent swaths and investigate the relationship between coverage width and various parameters, we have established both two-dimensional (2D) and three-dimensional (3D) geometric models to solve the parameters.

2.1. Two-Dimensional Multibeam Bathymetry Mathematical Model

2.1.1. Seawater Depth Model

Firstly, taking the measurement point as the coordinate origin, with the direction perpendicular to the sea surface as the y-axis and the rightward direction as the positive x-axis, we establish a Cartesian coordinate system as shown in Figure 1. In this representation, the seafloor is abstracted as a trapezoid.

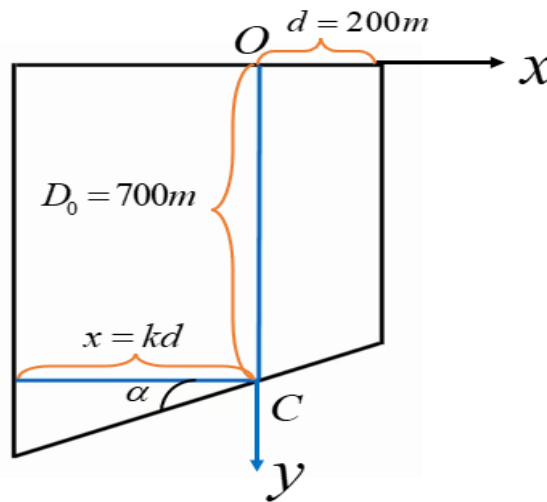


Figure 1: Trapezoidal Model of Seabed Depth

Let's denote the distance from the measurement line to the center point as kd , where k is an integer ($k = 0, \pm 1, \pm 2$). Point C is the intersection of the y-axis and the seabed slope surface, with coordinates $(kd, 0)$. Here, d is the distance (200m), D_0 is the initial depth (70m), and α is the slope. The x-coordinate of the intersection point of the measurement line with the x-axis is $x = kd$.

Analyzing the geometric relationships, we can derive the following equations:

If $k < 0$, then:

$$D = D_0 - kdtan\alpha \tag{1}$$

If $k > 0$, then:

$$D = D_0 + kdtan\alpha \tag{2}$$

2.1.2. Coverage Width Model

If the opening angle θ of the multibeam transducer is 120° and the slope is 1.5° , and assuming the swath intersects the seabed slope at points A and B, with the y-axis intersecting the seabed slope at point C, and a line l_1 passing through point A parallel to the y-axis intersects the swath at ϕ_1 , as shown in Figure 2 and Figure 3:

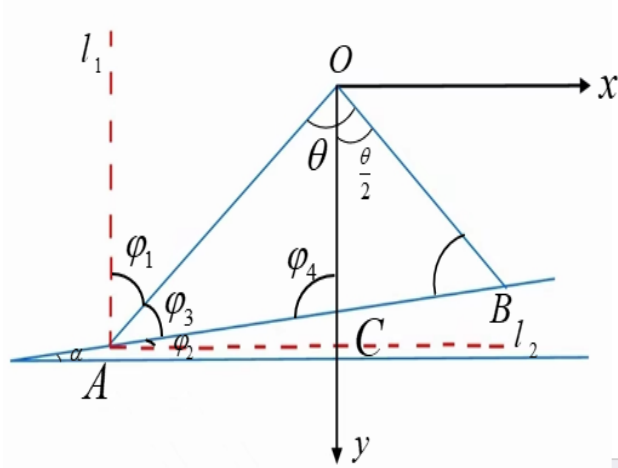


Figure 2: Schematic Diagram of Multibeam Transducer Bathymetry

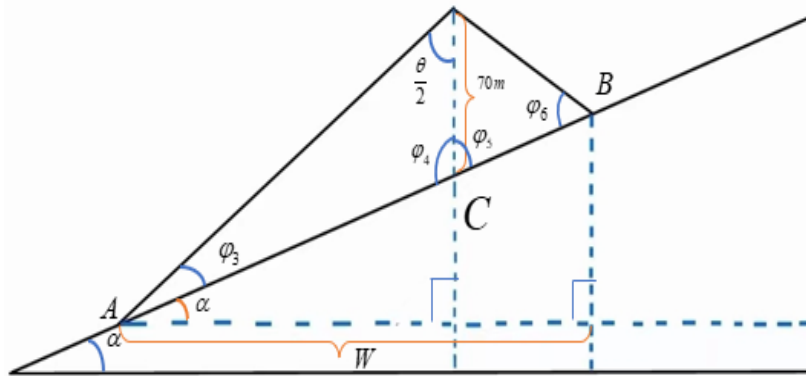


Figure 3: Schematic Diagram of Seabed Slope

According to the parallel property, we can have:

$$\phi_1 = \frac{\theta}{2} = 60^\circ. \tag{3}$$

Due to the fixed opening angle θ of the multibeam transducer being 120° and the slope α being 1.5° , the two angles ϕ_3 and ϕ_6 between the swath and the seabed slope are determined values. They do not change with variations in the seabed depth D . To calculate the coverage width, i.e:

$$W = (70 - kd \tan 1.5^\circ) \times \left(\frac{\sin 60^\circ}{\sin 28.5^\circ} + \frac{\sin 60^\circ}{\sin 31.5^\circ} \right) \times \cos \alpha. \tag{4}$$

2.2. Three-Dimensional Underwater Coverage Width Mathematical Model

2.2.1. Three-Dimensional Seawater Depth D

Establish a three-dimensional Cartesian coordinate system with the projection point O at the starting point of the ship as the origin. The direction of the normal projection is the y -axis, and the direction perpendicular to the sea surface is the z -axis, as illustrated in Figure 4.

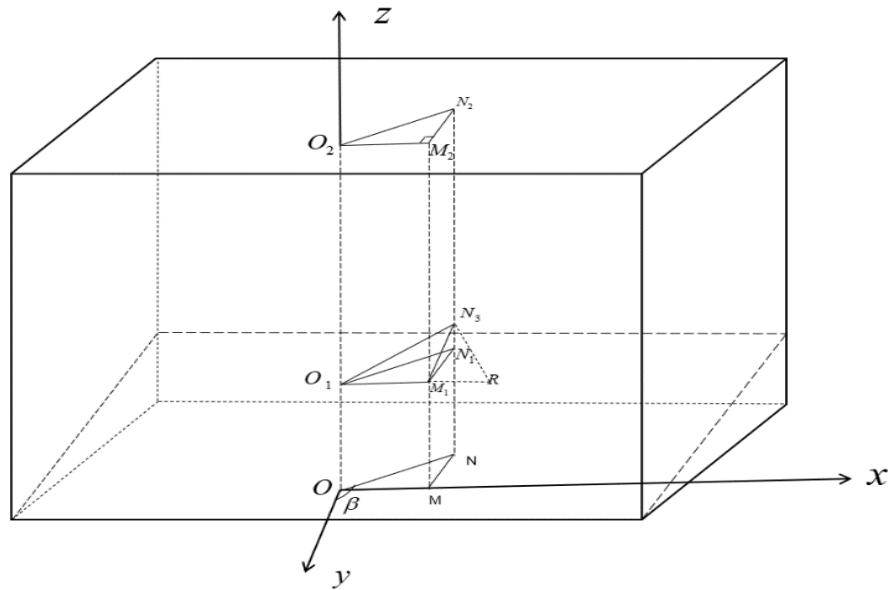


Figure 4: Three-Dimensional Schematic of the Sea Area

By the properties of projection, triangles OMN , $O_1M_1N_1$, and $O_2M_2N_2$ are congruent.

Segment O_1M_1 is the intersection line between the plane $O_1M_1N_1$ and the slope surface, meaning O_1M_1 lies on the slope surface. Triangle $O_1M_1N_3$ is then the projection of triangle $O_2M_2N_2$ on the slope surface. At this point, planes $O_1M_1N_1$ and $O_1M_1N_3$ form a dihedral angle, and the angle $\alpha = 1.5^\circ$. It follows that:

$$\angle MON = \angle M_1O_1N_1 = \beta - 90^\circ \tag{5}$$

The dihedral angle formed by the planes $O_1M_1N_1$ and $O_1M_1N_3$ is given by $\alpha = 1.5^\circ$. Therefore, we can conclude:

$$\angle N_1O_1M = \alpha = 1.5^\circ \tag{6}$$

$$M_1N_1 = O_1N_1 \times \tan\alpha = S \times \tan\alpha \tag{7}$$

From this, the seabed depth D can be determined:

$$D' = O_1O_2 = 120m \tag{8}$$

$$D = D' - S \times \tan\alpha \tag{9}$$

2.2.2. The Angle γ between the Trace of the Vertical Plane and the Slope Surface in the Horizontal Plane

Due to changes in the navigation direction, it affects the angle between the trace of the vertical plane and the intersection line with the slope surface in the horizontal plane. Given that the multibeam bathymetry swath is perpendicular to the direction of travel, with $ON_1 \perp N_1R$ and connecting to N_3R , the plane N_1RN_3 is part of the multibeam bathymetry swath. The angle between the trace of the vertical plane and the intersection line with the slope surface in the horizontal plane γ is equal to the angle N_1RN_3 . According to the definitions of similar triangles, we have:

$$\begin{aligned} N_1M_1 &= O_1N_1 \sin\angle N_1O_1M_1 = 1852 \times S \times \sin(\beta - 90^\circ) \\ O_1M_1 &= 1852 \times S \times \cos(\beta - 90^\circ) \end{aligned} \tag{10}$$

$$\begin{aligned} \tan \gamma &= \frac{N_1 R}{N_1 N_3} = \frac{1852 \times S \times \sin(\beta - 90^\circ) \times \tan \alpha}{1852 \times S \times \tan(\beta - 90^\circ)} \\ \gamma &= \arctan[\cos(\beta - 90^\circ) \tan \alpha] \\ &= \arctan \frac{\sin(\beta - 90^\circ) \tan \alpha}{\tan(\beta - 90^\circ)} \end{aligned} \tag{11}$$

2.2.3. Three-Dimensional Coverage Width *W*

According to formula (6), the slope α is influenced by the angle β between the direction of the measurement line and the normal projection of the seabed slope. This will refine the relationship for the coverage width W , where the distance of the measurement vessel from the center point of the sea area is denoted as s . Thus, we have:

$$W(S) = [D' - 1852 \times S \times \sin(\beta - 90^\circ) \times \tan \alpha] \times \left(\frac{\sin \frac{\theta}{2}}{\sin(90^\circ - \frac{\theta}{2} - \gamma)} + \frac{\sin \frac{\theta}{2}}{\sin(90^\circ - \frac{\theta}{2} + \gamma)} \right) \times \cos \gamma \tag{12}$$

2.3. Multibeam Survey Layout Optimization Model

Firstly, to obtain a bathymetric map of the sea area, visual processing is applied to the seawater depth data, as illustrated in Figure 5.

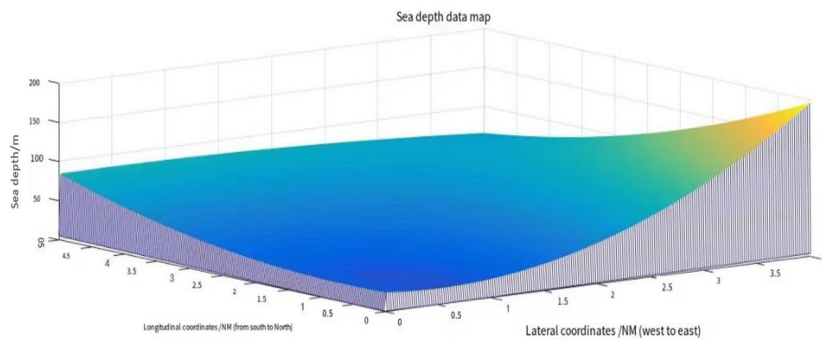


Figure 5: Bathymetric Data Visualization

Furthermore, the seabed is subdivided into dihedral slope surfaces along the northwest diagonal, simplifying and abstracting the bathymetric view from the top of the sea area. Considering practical scenarios, the goal is to minimize instances of missed measurements, aligning the route direction parallel to the slope bottom of the higher face. The coverage rate η is set to 10%.

At a depth $D = 65.2\text{m}$ on line AB , a point C_1 is selected at the same elevation as point C , and CC_1 is connected. At this point, CC_1 represents the direction of the measurement line, as shown in Figure 6.

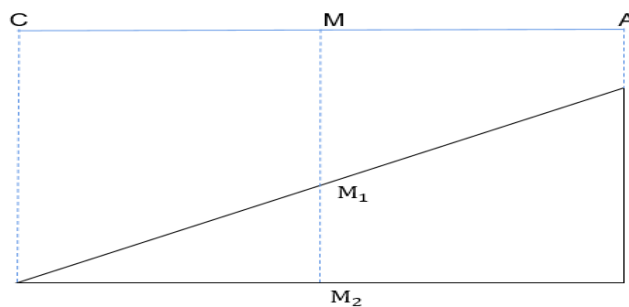


Figure 6: Longitudinal Sectional View of the Sea Area from West to East

Let's denote the depths as follows: $D_a=24.4\text{m}$ at point A , $D_b=84.4\text{m}$ at point B , $D_c=65.2\text{m}$ at point C , and $D_d=197.2\text{m}$ at point D . Using the following formula, we can calculate the angle γ between the trace

of the vertical plane and the intersection line with the slope surface in the horizontal plane at each point. Ultimately, this information helps determine the direction of the measurement line.

$$CE = \frac{CC_1}{\cos \varphi} \tag{13}$$

$$CM = CC_1 / \cos \angle \phi \tag{14}$$

$$\frac{M_1M_2}{D_{c1} - D_a} = \frac{CE}{AC} \tag{15}$$

$$\varphi = \arctan \left(\frac{MM_1}{C_1M} \right) \tag{16}$$

$$\gamma = \arctan \frac{\sin(\beta - 90^\circ) \tan \alpha}{\tan(\beta - 90^\circ)} \tag{17}$$

3. Results

For the two-dimensional multibeam bathymetry mathematical model, the calculated results for the parameters are presented in Table 1.

Table 1: Results Obtained from the Two-Dimensional Multibeam Bathymetry Mathematical Model

The distance of the measurement vessel from the center point/m	-800	-600	-400	-200	0	200	400	600	800
The seawater depth /m	90.9487	85.7116	80.4744	75.2372	70	64.7628	59.5256	54.2885	49.0513
The coverage width/m	315.7051	297.5256	279.3460	261.1665	242.9870	224.8074	206.6279	188.4484	170.2688
Overlap rate with the previous survey line./%	—	32.7789	28.4042	23.4205	17.6911	11.0350	3.2076	-6.1299	-17.4613

According to the three-dimensional seabed coverage width mathematical model, we have calculated the coverage width of multibeam bathymetry at different locations. The results are presented in Table 2.

Table 2: Coverage Width of Multibeam Bathymetry at Different Locations

The coverage width/m	The distance of the measurement vessel from the center point of the sea area/nautical miles								
	0	0.3	0.6	0.9	1.2	1.5	1.8	2.1	
The angle of the measurement line direction/°	0	415.692	466.091	516.49	566.889	617.288	667.687	718.086	768.484
	45	415.692	451.33	486.967	522.604	558.242	593.879	629.517	665.154
	90	416.549	416.549	416.549	416.549	416.549	416.549	416.549	416.549
	135	415.692	380.055	344.418	308.78	273.143	237.505	201.868	166.231
	180	415.692	365.293	314.895	264.496	214.097	163.698	113.299	62.9002
	225	415.692	380.055	344.418	308.78	273.143	237.505	201.868	166.231
	270	416.549	416.549	416.549	416.549	416.549	416.549	416.549	416.549
	315	415.692	451.33	486.967	522.604	558.242	593.879	629.517	665.154

In the multibeam survey layout optimization model, the calculated slope angle r is 0.39983871280891276. Consequently, the intersection points of each survey line with the y-axis can be computed. Based on this data, the total length of the survey lines is calculated as 573771.1610152135m. The estimated proportion of the total length occupied by the portion with an overlap rate exceeding 20% is approximately 30%.

4. Conclusion

In terms of measurement efficiency, multibeam bathymetry systems overcome the drawbacks of single-beam bathymetry. They can simultaneously emit multiple beams, enabling rapid and accurate measurement coverage while minimizing omissions. This significantly improves measurement efficiency compared to single-beam measurements, allowing for the quick completion of depth measurement tasks, especially in urgent situations. In terms of mapping, due to the ability to scan a larger number of water depth points, the system can more accurately reflect the seafloor conditions. During multibeam measurements, the scanning width changes continuously due to variations in water depth. The narrow scanning width of multibeam systems may require multiple scans back and forth. If shallow areas with unknown water depths suddenly appear during the scanning process, it can impede vessel navigation and potentially lead to damage to the multibeam probe. This jeopardizes the safety of exploration. Multibeam data collection is a dynamic process in complex marine environments, and the uncertainties and changes pose significant challenges and obstacles to both data acquisition and subsequent processing.

In summary, this paper analyzes the multibeam bathymetry problem and constructs a corresponding mathematical model. The model exhibits high reliability and practicality, suitable for visualizing the current status of underwater structures and studying the seafloor morphology near ocean ridges.

References

- [1] Brown, C. J., Smith, S. J., Lawton, P., & Anderson, J. T. (2011). *Benthic habitat mapping: A review of progress towards improved understanding of the spatial ecology of the seafloor using acoustic techniques*. *Estuarine, Coastal and Shelf Science*, 92(3), 502-520. <https://doi.org/10.1016/j.ecss.2011.02.007>
- [2] Mitchell, G. A., Orange, D. L., Gharib, J. J., & Kennedy, P. (2018). *Improved detection and mapping of deepwater hydrocarbon seeps: Optimizing multibeam echosounder seafloor backscatter acquisition and processing techniques*. *Marine Geophysical Research*, 39, 323-347. <https://doi.org/10.1007/s11001-018-9345-8>
- [3] Lucieer, V., Roche, M., Degrendele, K., Malik, M., Dolan, M., & Lamarche, G. (2018). *User expectations for multibeam echo sounders backscatter strength data-looking back into the future*. *Marine Geophysical Research*, 39, 23-40.
- [4] Hughes Clarke, J. E. (2016). *First wide-angle view of channelized turbidity currents links migrating cyclic steps to flow characteristics*. *Nature Communications*, 7, 11896. <https://doi.org/10.1038/ncomms11896>
- [5] Lamarche, G., Lurton, X., Verdier, A. L., & Augustin, J. M. (2011). *Quantitative characterisation of seafloor substrate and bedforms using advanced processing of multibeam backscatter-application to Cook Strait, New Zealand*. *Continental Shelf Research*, 31(2), S93-S109. <https://doi.org/10.1016/j.csr.2010.06.001>
- [6] Pratomo, D. G., & Saputro, I. (2021). *Comparative analysis of singlebeam and multibeam echosounder bathymetric data*. In *IOP Conference Series: Materials Science and Engineering* (Vol. 1052, No. 1, p. 012015). IOP Publishing. <https://doi.org/10.1088/1757-899X/1052/1/012015>
- [7] Weber, T. C., Rice, G., & Smith, M. (2018). *Toward a standard line for use in multibeam echo sounder calibration*. *Marine Geophysical Research*, 39, 75-87.
- [8] Parnum, I. M., & Gavrilov, A. N. (2011). *High-frequency multibeam echo-sounder measurements of seafloor backscatter in shallow water: Part 1-Data acquisition and processing*. *Marine Geophysical Research*, 32(1), 75-88. <https://doi.org/10.3723/ut.30.003>
- [9] Snellen, M., Gaida, T. C., Koop, L., Alevizos, E., & Simons, D. G. (2018). *Performance of multibeam echosounder backscatter-based classification for monitoring sediment distributions using multi-temporal large-scale ocean data sets*. *Marine Geophysical Research*, 39(1-2), 17-32. <https://doi.org/10.1109/JOE.2018.2791878>
- [10] Roche, M., Degrendele, K., Vrignaud, C., Loyer, S., Le Bas, T., Augustin, J. M., & Lurton, X. (2018). *Control of the repeatability of high frequency multibeam echosounder backscatter by using natural reference areas*. *Marine Geophysical Research*, 39, 89-104. <https://doi.org/10.1007/s11001-018-9343-x>